Published in final edited form as:
Eur J Nucl Med Mol Imaging. 2010 October ; 37(10): 1943–1949. doi:10.1007/s00259-010-1447-8.

Biodistribution and radiation dosimetry of a positron emission tomographic ligand, ^{18}F-SP203, to image metabotropic glutamate subtype 5 receptors in humans

Yasuyuki Kimura,
Molecular Imaging Branch, National Institute of Mental Health, 10 Center Drive, Bethesda, MD 20892-1026, USA

Fabrice G. Siméon,
Molecular Imaging Branch, National Institute of Mental Health, 10 Center Drive, Bethesda, MD 20892-1003, USA

Jun Hatazawa,
Department of Nuclear Medicine and Tracer Kinetics, Osaka University Graduate School of Medicine, Suita, Osaka, Japan

P. David Mozley,
Merck Research Laboratories, West Point, PA, USA

Victor W. Pike,
Molecular Imaging Branch, National Institute of Mental Health, 10 Center Drive, Bethesda, MD 20892-1003, USA

Robert B. Innis, and
Molecular Imaging Branch, National Institute of Mental Health, 10 Center Drive, Bethesda, MD 20892-1026, USA

Masahiro Fujita
Molecular Imaging Branch, National Institute of Mental Health, 10 Center Drive, Bethesda, MD 20892-1026, USA

Abstract

Purpose—A new PET ligand, 3-fluoro-5-(2-(2-^{18}F-(fluoromethyl)-thiazol-4-yl)ethynyl)benzonitrile (^{18}F-SP203), is a positron emission tomographic radioligand selective for metabotropic glutamate subtype 5 receptors. The purposes of this study were to estimate the radiation-absorbed doses of ^{18}F-SP203 in humans and to determine from the distribution of radioactivity in bone structures with various proportions of bone and red marrow whether ^{18}F-SP203 undergoes defluorination.

Methods—Whole-body images were acquired for 5 h after injecting ^{18}F-SP203 in seven healthy humans. Urine was collected at various time points. Radiation-absorbed doses were estimated by the Medical Internal Radiation Dose scheme.

Results—After injecting ^{18}F-SP203, the two organs with highest radiation exposure were urinary bladder wall and gallbladder wall, consistent with both urinary and fecal excretion. In the skeleton, most of the radioactivity was in bone structures that contain red marrow and not in those without

fujitam@mail.nih.gov .

Conflict of interest None.

red marrow. Although the dose to red marrow (30.9 μSv/MBq) was unusually high, the effective dose (17.8 μSv/MBq) of ^{18}F-SP203 was typical of that of other ^{18}F radiotracers.

Conclusion—^{18}F-SP203 causes an effective dose in humans typical of several other ^{18}F radioligands and undergoes little defluorination.

Keywords

mGluR5; PET; Dosimetry; Defluorination

Introduction

The metabotropic glutamate subtype 5 receptor (mGluR5) is a G-protein-coupled receptor that is predominantly expressed postsynaptically, and is located in several brain regions, including the striatum, hippocampus, amygdala, and cortex [1]. A PET radioligand for mGluR5 may be useful to assess its dysfunction in brain diseases and to develop new therapeutic drugs. Two PET radioligands for mGluR5 have been tested in humans: ^{11}C-ABP688 [2] and ^{18}F-SP203 [3]. Both are negative allosteric modulators; that is, they oppose the intracellular signaling cascade (phospholipase C and phosphoinositide hydrolysis) stimulated by glutamate but at a site on mGluR5 other than the binding site of glutamate itself.

Ametamey et al. [4] developed the first radioligand, ^{11}C-ABP688, used in human subjects, and demonstrated full quantification of brain uptake relative to serial concentrations of parent radioligand in arterial plasma [2]. Merck developed another ligand, ^{18}F-MTEB, and reported studies in monkeys [5] but have not yet reported studies in humans. We also developed one other PET ligand, ^{18}F-SP203 [6], and fully quantified its binding in human brain relative to serial concentrations of parent radioligand in arterial plasma [3]. Our ligand has several advantages compared to the previously reported ligands. First, the longer half-life of ^{18}F easily allows distribution of the ligand to other facilities. Second, ^{18}F-SP203 shows higher peak uptake in human brain than ^{11}C-ABP688. As a disadvantage of our ligand, a moderate amount of radioactivity accumulation in the skull has been seen at late time points in human brain imaging [3]. Radioactivity in the skull may reflect the presence of ^{18}F ion in bone and/or radioactivity (parent radioligand or other radiometabolites) in red marrow, because the skull contains both bone and red marrow.

The purposes of this study were to estimate the radiation-absorbed doses of ^{18}F-SP203 in humans and to determine from the peripheral distribution of radioactivity whether ^{18}F-SP203 undergoes defluorination. By studying the distribution of radioactivity in bone structures in the entire body with various compositions of bones and red marrow, relative accumulation of radioactivity in bone and red marrow can be estimated.

Materials and methods

Radioligand preparation

^{18}F-SP203 was prepared from the bromomethyl analog of SP203 and ^{18}F fluoride ion, as previously described [6]. The preparation is described in detail in our Investigational New Drug Application 78,260, a copy of which is available at http://pdsp.med.unc.edu/snidd/. For studies in humans, ^{18}F-SP203 had a radiochemical purity of >98% and specific activity at the time of injection of 101±89 GBq/μmol (n=4 preparations).

Subjects

Three female and four male healthy volunteers were enrolled (body weight 72.6±5.7 kg, age 25.2±5.3 years). All subjects were free of medical or neuropsychiatric illnesses on the basis of a history, physical examination, electrocardiogram, and standard blood and urine analyses, which included a complete blood count, serum chemistry, thyroid function test, urinalysis, urine drug screen, as well as syphilis, HIV, and hepatitis B screenings. Our use of ^{18}F-SP203 in human subjects was approved by the Radiation Safety Committee of the National Institutes of Health and the Institutional Review Board of the National Institute of Mental Health. This study was performed in accordance with the ethical standards laid down in the 1964 Declaration of Helsinki. All subjects gave their informed consent prior to their inclusion in the study.

PET scans

After intravenous injection of ^{18}F-SP203 (141±41 MBq), 2-D dynamic whole-body PET images were acquired on a GE Advance tomograph (GE Medical Systems, Waukesha, WI). We followed the procedure for image acquisition and reconstruction described previously by our group [7]. In brief, each subject was imaged in seven contiguous 15-cm bed positions (head to upper thigh) in 16 frames, each of increasing duration (15 s to 4 min) for a total scan time of 300 min. All PET images were reconstructed with ordered subset expectation maximization image reconstruction and were corrected for attenuation and scatter. Subjects had three rest periods (30 min each) outside the camera, beginning at approximately 120, 180, and 240 min after injection of the radioligand. Blood pressure, pulse rate, respiration rate, and an electrocardiogram were obtained before and 15, 30, 90, 120, and 180 min after the injection.

Image analysis

Brain, lungs, heart, liver, kidneys, gallbladder, urinary bladder, and skeleton were visually identifiable as source organs (Fig. 1). Large regions were placed to encompass all accumulated radioactivity in each organ. For each organ, we chose the most visible frame to draw the region and applied it to the remaining frames. When organs showed an apparent movement from the place in the frame used to place the drawing on the regions, we manually moved the regions with the same shape to fit them to the organ in the new place.

In the skeleton, red marrow is primarily located in the ribs, vertebrae, and pelvis but not in the distal limbs [8, 9]. We found uptake in the bone structures that contain red marrow, but marrow-poor diaphyses of the tubular bones were not visible. Thus, all uptake in the skeleton was assumed to have derived from red marrow.

Regions were placed on the tomographic images in two ways based upon the amount of radioactivity and the visibility of the source organ. First, for organs with high uptake (brain, kidneys, liver, gallbladder, urinary bladder, and lumbar vertebrae), regions were drawn on each coronal slice in which the organ was visible. Second, for organs with low uptake (heart, spleen, and lungs), regions were drawn on summed slices to increase the contrast with surrounding tissue. To avoid contamination of activity in the left lung by activity in the heart, activity was measured only in the right lung and then multiplied by the ratio of the right lung mass to the total lung mass (1:1.87) [10]. Images were analyzed using PMOD 2.95 software (PMOD Technologies, Zurich, Switzerland).

Calculating residence times

The residence time in each source organ was calculated as the area under the curve of time–activity curve, which was created after removing decay correction and applying recovery correction. The area under the curve to the end of imaging was calculated by the trapezoidal

method, and from the end to infinity was calculated by assuming that further decline in radioactivity occurred only by physical decay without any biological clearance. The area under the curve of the fraction of measured injected activity from time zero to infinity is equivalent to the residence time. The recovery correction was applied based on the activity of the first frame in the body above the thigh measured by PET, which was 98±3% of the injected activity measured using a dose calibrator. The time–activity curves were created with time information of the bed position in which the source organ was primarily included when the organ was not confined to a single bed position.

The residence time of all red marrow in the body was estimated from that of the lumbar vertebrae. A small proportion of radioactivity in the lumbar vertebrae may come from bone, but not from red marrow. To estimate radiation-absorbed doses in a conservative way, we assigned all radioactivity in the lumbar vertebrae to red marrow. Because the mass of red marrow in the lumbar vertebrae is 11.7% of the mass of all red marrow in the body [8, 9], the residence time in red marrow in the entire body was calculated by multiplying that of the lumbar vertebrae by 100/11.7.

To calculate the residence time of the remainder of the body, the residence time of all source organs was summed and subtracted from the fixed theoretical value of $T_{1/2}/\ln 2$, which equals 2.640 h for ^{18}F.

Urinary excretion

We used the dynamic urinary bladder model with a voiding interval of 2.4 h to calculate the residence time in the bladder [11]. Urine was collected for 17 to 21 h in four subjects and for 5 h in three subjects. The total activity in the urine was added to that measured in the urinary bladder in the PET scan to determine total radioactivity excreted after injection. The cumulative urine activity curve was decay-corrected and expressed as a fraction of injected activity. This curve from all subjects was fitted to a monoexponential and a biexponential function, and the function that identified parameters was chosen to estimate total radioactivity excreted at infinite time.

Estimation of absorbed radiation doses

Radiation absorbed doses were calculated based on the Medical Internal Radiation Dose scheme by entering the average residence time of seven subjects for each source organ into OLINDA 1.0/EXM software [12] for a 70-kg adult male.

Results

The injected activity of ^{18}F-SP203 was 141±41 MBq, which corresponds to 1.9±1.0 nmol SP203 (a total of seven injections in seven subjects). The injected dose of ^{18}F-SP203 caused no pharmacological effects during the 5-h scan, based on subject reports, ECG, blood pressure, pulse rate, and respiration rate. In addition, no effects were noted in any of the blood and urine tests acquired 7 to 24 h after radioligand injection.

Brain, heart, lungs, liver, spleen, gallbladder, kidneys, skeleton, and urinary bladder were visually identified on the images and treated as source organs of radioactivity for dosimetry calculations (Fig. 1). The liver had the highest uptake, with a peak of 13% of injected activity at about 4 min. The peak uptakes in other organs were 11% in brain, 9.1% in kidneys, 4.7% in lungs, 3.4% in heart, and 1.9% in spleen, all of which occurred within 8 min of injection (Fig. 2). Radioactivity slowly accumulated in the gallbladder (0.9%) and red marrow (14%), reaching an asymptote within 100 min (Fig. 2).

Radioactivity in the images of the urinary bladder was combined with that directly measured in the urine and fitted to biexponential and monoexponential functions. Because the biexponential fit did not identify the parameters, the monoexponential function was used for the dosimetry calculation (Fig. 3). This curve indicated that 33% of injected radioactivity was excreted via the urine at infinite time, with a biological half-life of 2.8 h. The amount of radioactivity excreted via the feces could not be determined from this imaging study that lasted for only 5 h. However, the gallbladder was clearly visible in all subjects and its radioactivity reached a maximum of 0.9% injected activity within about 100 min. The small intestine was not visualized, which may suggest that the radioactivity was reabsorbed via the enterohepatic circulation.

The organs with the longest residence time were the red marrow (0.307 h), brain (0.192 h), and liver (0.091 h). The source organs with lower residence times were the lungs (0.065 h), heart (0.024 h), gallbladder (0.018 h), and spleen (0.014 h) (Table 1). Based on a 2.4-h interval for urinary voiding, the organs with the highest radiation doses were: urinary bladder wall (76.0 μSv/MBq), gallbladder wall (39.8 μSv/MBq), brain (34.5 μSv/MBq), and red marrow (30.9 μSv/MBq) (Table 2). The effective dose was 17.8 μSv/MBq.

Discussion

Whole-body scans of ^{18}F-SP203 showed that radiation absorbed doses of ^{18}F-SP203 in humans were similar to those of other ^{18}F-labeled tracers. Based on the biodistribution data in human subjects, we estimated the radiation burden of ^{18}F-SP203 to have an effective dose of 17.8 μSv/ MBq, which would allow multiple scans in the same individual under two of the three major guidelines and at least one scan under more stringent guidelines. Although the dose to red marrow (30.9 μSv/MBq) from ^{18}F-SP203 was higher than that from other ^{18}F-labeled tracers, the effective doses were similar (Table 3). Based on the distribution of radioactivity in bone structures with various levels of red marrow, the majority of activity in the human skeleton was in the red marrow rather than in bone itself, and ^{18}F-SP203 undergoes little defluorination in humans. Thus, the uptake in the skull, which we found in a previous study [3], reflects primarily uptake in red marrow.

Effect of organ doses on maximal injected activity

Limits of radiation exposure in research subjects vary, and there are three commonly used guidelines in the world. First, the guidelines of the Radioactive Drug Research Committees operating in the USA under the auspices of the Food and Drug Administration have limits for both effective dose and dose to individual organs, whichever occurs first [13]. The dose limits for adults are 30 mSv per single administration and 50 mSv per year to the whole body, lens of the eye, red bone marrow, and gonads, and 50 mSv per single administration and 150 mSv per year to all other organs. With these limits, the maximal injectable activity would be 0.7 GBq per single administration based on the dose to the urinary bladder wall and 1.6 GBq per year based on the dose to the red marrow. The guidelines of the National Institutes of Health have a limit for the effective dose of 50 mSv per year (http://drs.ors.od.nih.gov/services/rsc/forms_index.htm). Based on this limit, the maximal injectable activity is 2.8 GBq per year. Most countries in Europe allow a maximum dose that causes a “minor to intermediate” increase of risk, which represents an effective dose limit of 10 mSv per year [14]. Thus, research subjects in Europe could receive no more than 562 MBq ^{18}F-SP203 per year. Because we have reported that injection activity of about 320 MBq allows accurate measurement of ^{18}F-SP203 binding to mGluR5 in brain [3], the radiation absorbed doses reported in the current study allow multiple scans under two of the three guideline and at least one scan under the strictest guideline used in Europe.

The most important source of error in the estimation of the radiation absorbed doses could be the definition of volume of interest. In this study, we assumed that all uptake in the skeleton was derived from red marrow because only the bone structures that contain red marrow were visible on PET images. If there is a small activity in bone itself, the absorbed dose to red marrow and eventually the effective dose might be overestimated. However, possible overestimation is preferable to underestimation because overestimation would prevent giving too much activity of ^{18}F-SP203 to subjects.

Defluorination

The ^{18}F-fluoride ion resulting from systemic metabolism of radioligands accumulates in bone, and the uptake in the skull may spill into adjacent brain and artificially elevate measured radioactivity [15]. In our previous brain imaging study with ^{18}F-SP203, we found moderate uptake of radioactivity in the skull and interpreted it as the result of systemic metabolism and uptake of ^{18}F-fluoride ion into the bone of the skull [3]. However, in the current study, most of the radioactivity was in bone structures that contain red marrow and not in bones without red marrow. Thus, the uptake in the skull, which we found in the previous study, reflects uptake in primarily red marrow, and ^{18}F-SP203 undergoes little defluorination in humans.

We do not know the chemical identity of the radioactivity in the red marrow, but it could be ^{18}F-fluoride ion, as it is in bone. We have previously determined that ^{18}F-SP203 is defluorinated in rat brain, both in vitro and in vivo, via glutathione S-transferase [16]. The resulting ^{18}F-fluoride ion is trapped in the brain because of its negative charge. The activity and forms of glutathione S-transferase vary across species and within organs of the same species [17, 18]. Fortunately, monkey and human brains may contain negligible levels of glutathione S-transferase and do not generate ^{18}F-fluoride ion during in vitro incubation with ^{18}F-SP203 [6]. The cause of high radioactivity in red marrow is unknown. However, its chemical identity is not unmetabolized ^{18}F-SP203 but the radiometabolites. Our preliminary experiments in monkeys showed that radioactivity in red marrow was markedly decreased by ^{18}F labeling at different positions. ^{18}F-SP203 has the ^{18}F labeling at the alkyl position. Labeling at the aryl position instead of the alkyl position markedly decreased bone marrow activity. Thus, the radioactivity in red marrow is not from specific binding or nonspecific binding of ^{18}F-SP203, but from radiometabolites. Because aryl carbonfluorine bonds are generally more resistant to defluorination in vivo than alkyl carbon–fluorine bonds, we speculate that the ^{18}F-fluoride ion, which is generated by glutathione S-transferase in red marrow is trapped intracellularly leading to the higher absorbed dose in red marrow than that of other ^{18}F-labeled radioligands.

Conclusion

^{18}F-SP203 is an effective ligand for the imaging of mGluR5 and its effective dose in humans is typical of that of other ^{18}F-labeled radiotracers. ^{18}F-SP203 undergoes little defluorination in humans. Depending upon local guidelines for radiation exposure to research subjects, the high radiation burden to the red marrow may limit the amount of injectable radioactivity.

Acknowledgments

This research was supported by the Intramural Program of the National Institute of Mental Health (projects Z01-MH-002795-07 and Z01-MH-002852-04). We thank Leah P. Dickstein, Maria D. Ferraris Araneta, Gerald L. Hodges, Nobuyo Kimura, Barbara Scepura, Cheryl Wallisch, Yi Zhang, Jeih-San Liow, Robert L. Gladding, Amira K. Brown, and the staff of the PET Department for successful completion of the studies; and Dr. Michael G. Stabin for his suggestions concerning the data analysis; and PMOD Technologies (Zurich, Switzerland) for providing its image analysis and modeling software.

References

1. Kenny PJ, Markou A. The ups and downs of addiction: role of metabotropic glutamate receptors. Trends Pharmacol Sci. 2004; 25:265–72. [PubMed: 15120493]
2. Ametamey SM, Treyer V, Streffer J, Wyss MT, Schmidt M, Blagoev M, et al. Human PET studies of metabotropic glutamate receptor subtype 5 with ^{11}C-ABP688. J Nucl Med. 2007; 48:247–52. [PubMed: 17268022]
3. Brown AK, Kimura Y, Zoghbi SS, Siméon FG, Liow JS, Kreisl WC, et al. Metabotropic glutamate subtype 5 receptors are quantified in the human brain with a novel radioligand for PET. J Nucl Med. 2008; 49:2042–8. [PubMed: 19038998]
4. Ametamey SM, Kessler LJ, Honer M, Wyss MT, Buck A, Hintermann S, et al. Radiosynthesis and preclinical evaluation of ^{11}C-ABP688 as a probe for imaging the metabotropic glutamate receptor subtype 5. J Nucl Med. 2006; 47:698–705. [PubMed: 16595505]
5. Hamill TG, Krause S, Ryan C, Bonnefous C, Govek S, Seiders TJ, et al. Synthesis, characterization, and first successful monkey imaging studies of metabotropic glutamate receptor subtype 5 (mGluR5) PET radiotracers. Synapse. 2005; 56:205–16. [PubMed: 15803497]
6. Siméon FG, Brown AK, Zoghbi SS, Patterson VM, Innis RB, Pike VW. Synthesis and simple ^{18}F-labeling of 3-fluoro-5-(2-(2-(fluoromethyl)thiazol-4-yl)ethynyl)benzonitrile as a high affinity radioligand for imaging monkey brain metabotropic glutamate subtype-5 receptors with positron emission tomogra-phy. J Med Chem. 2007; 50:3256–66. [PubMed: 17571866]
7. Sprague DR, Chin FT, Liow JS, Fujita M, Burns HD, Hargreaves R, et al. Human biodistribution and radiation dosimetry of the tachykinin NK1 antagonist radioligand [^{18}F]SPA-RQ: comparison of thin-slice, bisected, and 2-dimensional planar image analysis. J Nucl Med. 2007; 48:100–7. [PubMed: 17204705]
8. Cristy M. Active bone marrow distribution as a function of age in humans. Phys Med Biol. 1981; 26:389–400. [PubMed: 7243876]
9. The International Commission on Radiological Protection. Basic anatomical and physiological data: the skeleton. ICRP Publication 70 Ann ICRP. 1995; 25:1–80.
10. The International Commission on Radiological Protection. Basic anatomical and physiological data for use in radiological protection: reference values. ICRP Publication 89. Ann ICRP. 2002; 32:1–277.
11. Cloutier RJ, Smith SA, Watson EE, Snyder WS, Warner GG. Dose to the fetus from radionuclides in the bladder. Health Phys. 1973; 25:147–61. [PubMed: 4784245]
12. Stabin MG, Sparks RB, Crowe E. OLINDA/EXM: the second-generation personal computer software for internal dose assessment in nuclear medicine. J Nucl Med. 2005; 46:1023–7. [PubMed: 15937315]
13. Code of Federal Regulations. Title 21: Food and Drugs. Chapter 1 - Food and Drug Administration, Department of Health and Human Services. Part 361 - Prescription drugs for human use generally recognized as safe and effective and not misbranded: drugs used in research. Sect. 361.1: Radioactive drugs for certain research uses. 2010.
14. International Commission on Radiological Protection. Radiological protection in biomedical research. ICRP Publication 62. Ann ICRP. 1993; 22:A1.
15. Ryu YH, Liow JS, Zoghbi S, Fujita M, Collins J, Tipre D, et al. Disulfiram inhibits defluorination of ^{18}F-FCWAY, reduces bone radioactivity, and enhances visualization of radioligand binding to serotonin 5-HT$_{1A}$ receptors in human brain. J Nucl Med. 2007; 48:1154–61. [PubMed: 17574977]
16. Shetty HU, Zoghbi SS, Simeon FG, Liow JS, Brown AK, Kannan P, et al. Radiodefluorination of 3-fluoro-5-(2-(2-[^{18}F](fluoromethyl)-thiazol-4-yl)ethynyl)benzonitrile ([^{18}F]SP203), a radioligand for imaging brain metabotropic glutamate subtype-5 receptors with positron emission tomography, occurs by glutathionylation in rat brain. J Pharmacol Exp Ther. 2008; 327:727–35. [PubMed: 18806125]
17. Bogaards JJ, Venekamp JC, Salmon FG, van Bladeren PJ. Conjugation of isoprene monoepoxides with glutathione, catalyzed by α, μ, π and θ-class glutathione S-transferases of rat and man. Chem Biol Interact. 1999; 117:1–14. [PubMed: 10190541]

18. Cannady EA, Chien C, Jones TM, Borel AG. In vitro metabolism of the epoxide substructure of cryptophycins by cytosolic glutathione S-transferase: species differences and stereoselectivity. Xenobiotica. 2006; 36:659–70. [PubMed: 16891247]

19. Vesselle H, Grierson J, Peterson LM, Muzi M, Mankoff DA, Krohn KA. ^{18}F-Fluorothymidine radiation dosimetry in human PET imaging studies. J Nucl Med. 2003; 44:1482–8. [PubMed: 12960196]

20. Zanzonico PB, Finn R, Pentlow KS, Erdi Y, Beattie B, Akhurst T, et al. PET-based radiation dosimetry in man of ^{18}F-fluorodihydrotestosterone, a new radiotracer for imaging prostate cancer. J Nucl Med. 2004; 45:1966–71. [PubMed: 15534070]

21. Deterding TA, Votaw JR, Wang CK, Eshima D, Eshima L, Keil R, et al. Biodistribution and radiation dosimetry of the dopamine transporter ligand [^{18}F]FECNT. J Nucl Med. 2001; 42:376–81. [PubMed: 11216538]

22. Koole M, Lewis DM, Buckley C, Nelissen N, Vandenbulcke M, Brooks DJ, et al. Whole-body biodistribution and radiation dosimetry of ^{18}F-GE067: a radioligand for in vivo brain amyloid imaging. J Nucl Med. 2009; 50:818–22. [PubMed: 19372469]

23. Obrzut SL, Koren AO, Mandelkern MA, Brody AL, Hoh CK, London ED. Whole-body radiation dosimetry of 2-[^{18}F]fluoro-A-85380 in human PET imaging studies. Nucl Med Biol. 2005; 32:869–74. [PubMed: 16253812]

24. Brown WD, Oakes TR, DeJesus OT, Taylor MD, Roberts AD, Nickles RJ, et al. Fluorine-18-fluoro-L-DOPA dosimetry with carbidopa pretreatment. J Nucl Med. 1998; 39:1884–91. [PubMed: 9829576]

25. Robeson W, Dhawan V, Belakhlef A, Ma Y, Pillai V, Chaly T, et al. Dosimetry of the dopamine transporter radioligand ^{18}F-FPCIT in human subjects. J Nucl Med. 2003; 44:961–6. [PubMed: 12791826]

26. Deloar HM, Fujiwara T, Shidahara M, Nakamura T, Watabe H, Narita Y, et al. Estimation of absorbed dose for 2-[F-18]fluoro-2-deoxy-D-glucose using whole-body positron emission tomography and magnetic resonance imaging. Eur J Nucl Med. 1998; 25:565–74. [PubMed: 9618570]

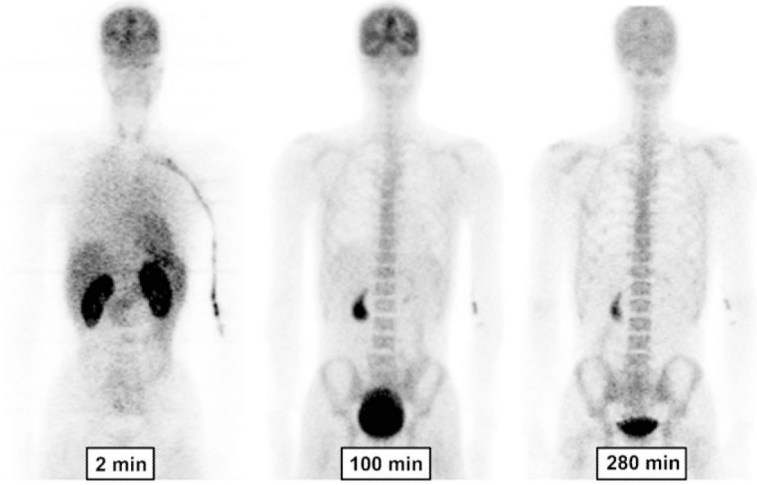

Fig. 1.
Whole-body images of a healthy man at about 2, 100, and 280 min after injection of ^{18}F-SP203 (196 MBq). The images are decay-corrected and displayed using the same gray scale. All coronal slices of each time-point were summed to create the images

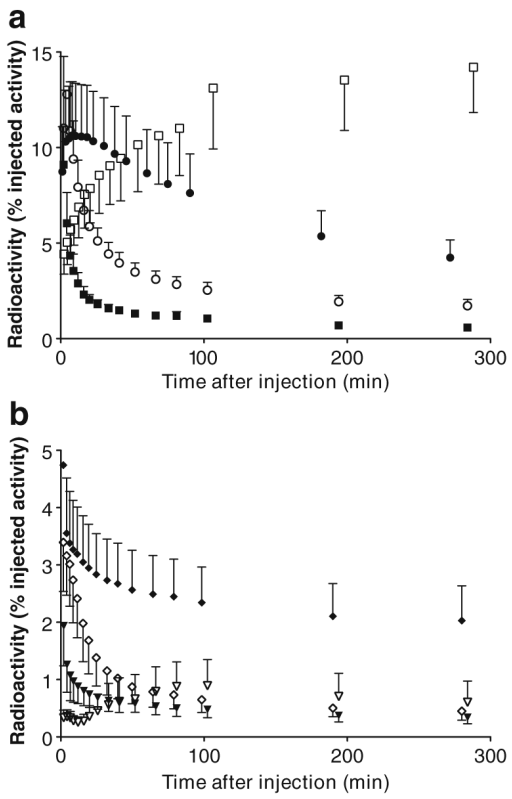

Fig. 2.

Time-activity curves for source organs with high (a) and low (b) uptake of radioactivity after injection of ^{18}F-SP203 in seven healthy humans. Symbols represent the mean, and error bars reflect SD. a ● brain, ○ liver, ■ kidney, and □ red marrow. b ◆ lungs, ◇ heart, ▼ spleen, and ▽ gallbladder. The error bar of the peak time points for liver (12.8±3.4% injected activity at 4.3 min) and lung (4.7±1.5% injected activity at 1.8 min) are omitted because their high values would have unnecessarily extended the *y*-axis

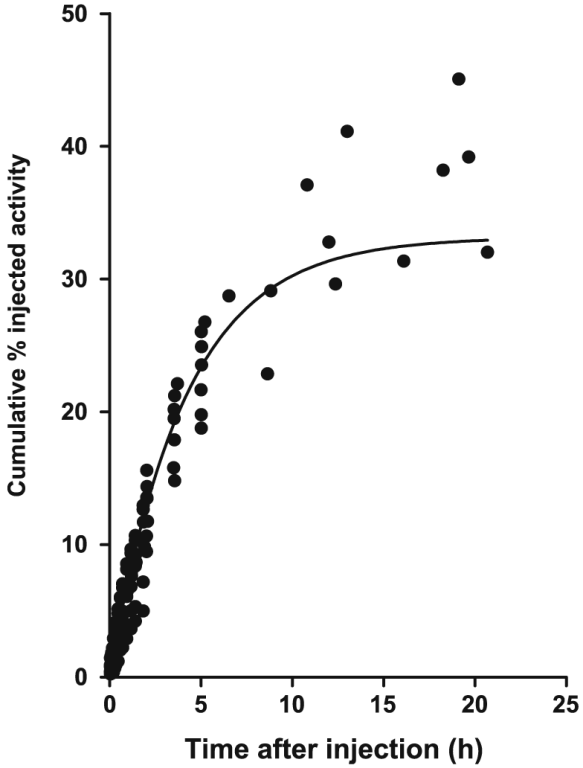

Fig. 3.

Cumulative urine activity measured from PET images and urine collection. The data were derived from all subjects and are corrected for radioactive decay. The solid line is a monoexponential curve with an asymptote of 33% and a half-life of 2.8 h. The asymptote and the biological half-life were used for the dynamic bladder model, with a voiding interval of 2.4 h, to calculate radiation dose

Table 1

Residence times of source organs determined from whole-body imaging of seven healthy subjects injected with ^{18}F-SP203 Values are means±SD

Organ	Residence time (h)
Brain	0.192±0.048
Lungs	0.065±0.017
Heart	0.024±0.008
Liver	0.091±0.015
Spleen	0.014±0.004
Kidney	0.037±0.004
Gallbladder	0.018±0.009
Red marrow	0.307±0.063
Remainder of body	1.585±0.147

Table 2

Radiation dosimetry estimates for ^{18}F-SP203 in standard reference man

Organ	Radiation dose	
	μSv/MBq	mrem/mCi
Adrenals	12.7	47.0
Brain	34.5	127.0
Breasts	7.6	28.2
Gallbladder wall	39.8	147.0
Lower large intestine wall	12.8	47.4
Small intestine	12.1	44.8
Stomach wall	10.6	39.1
Upper large intestine wall	11.7	43.4
Heart wall	20.1	74.2
Kidneys	29.4	109.0
Liver	16.2	60.0
Lungs	16.6	61.5
Muscle	9.4	34.9
Ovaries	13.1	48.4
Pancreas	12.5	46.3
Red marrow	30.9	114.0
Osteogenic cells	25.8	95.3
Skin	7.1	26.4
Spleen	20.5	75.7
Testes	9.3	34.4
Thymus	9.6	35.5
Thyroid	9.6	35.3
Urinary bladder wall[a]	76.0	281.0
Uterus	15.0	55.5
Total body	11.3	41.7
Effective dose	17.8	65.7

[a]Determined from the dynamic urinary bladder model with a voiding interval of 2.4 h.

Table 3

Radiation dose to red marrow and effective dose of various ^{18}F-labeled radioligands

Radioligand	Dose to red marrow (μSv/MBq)	Effective dose (μSv/MBq)	Reference
^{18}F-SP203	30.9	17.8	Current study
^{18}F-Fluorothymidine	24.0	15.5[a]	[19]
^{18}F-Fallypride	19.5	21.1	Communication from R.M. Kessler
^{18}F-Fluorodihydrotestosterone	18.7	12.5[a]	[20]
^{18}F-FECNT	16.1	15.8	[21]
^{18}F-SPARQ	15.8	29.3	[7]
^{18}F-GE067	15.3	33.8	[22]
^{18}F-Fluoro-A-85380	14.1	23.7	[23]
^{18}F-FDOPA	10.5	19.9	[24]
^{18}F-FPCIT	5.1	8.6[a]	[25]
^{18}F-FDG	5.0	29.0	[26]

[a] Approximate effective dose calculated from the reported doses of individual organs.